Journal of Power Sources 252 (2014) 113–121

Contents lists available at ScienceDirect

Journal of Power Sources

journal homepage: www.elsevier.com/locate/jpowsour

Larger-scale fabrication of N-doped graphene-fiber mats used in high-performance energy storage

Yunzhen Chang, Gaoyi Han*, Dongying Fu, Feifei Liu, Miaoyu Li, Yanping Li

Institute of Molecular Science, Key Laboratory of Chemical Biology and Molecular Engineering of Education Ministry, Shanxi University, Taiyuan 030006, China

HIGHLIGHTS

- The N-doped graphene fiber mats (NG-FMs) have been fabricated by wet spinning GO.
- NG-FMs are flexible and possess pores with the larger interior and small entrance.
- Capacitors assembled by NG-FMs possess high-rate capability and excellent stability.

GRAPHICAL ABSTRACT

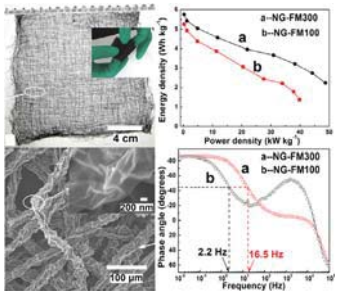

ARTICLE INFO

Article history:
Received 31 August 2013
Received in revised form
27 October 2013
Accepted 29 November 2013
Available online 10 December 2013

Keywords:
Graphene
Fiber
N-doped
Capacitors

ABSTRACT

The N-doped graphene fibers mats (NG-FMs) have been fabricated through spinning GO into ethanol solution of hydroxylamine and following thermal treatment. The NG-FMs are flexible and possess pores with the large interior and small entrance. The results of characterization indicate that N has doped into the graphene sheets during the preparation of the fibers, and that the interplanar distance of the graphene sheets in the fibers has almost no change with the increase of the treating temperature. The capacitive properties of the NG-FMs have been investigated by electrochemical method using two-electrode symmetric capacitor test. The results show that the specific capacitance of NG-FMs can reach 188 F g^{-1} at scan rate of 5 mV s^{-1} and the capacitors assembled by them possess the high-rate capability (the impedance phase angle can reach −45° at 16.5 Hz) and good cycling stability. The energy density and power density of the capacitor can reach to 2.24 Wh kg^{-1} and 48.7 kW kg^{-1} at discharged current density of 300 A g^{-1} (excluding *iR* drop).

1. Introduction

Electrochemical capacitors are considered as excellent electrical energy storage devices because their higher power density than rechargeable batteries and much greater capacitance than conventional dielectric capacitors [1–4]. Based on the energy storage mechanisms, the capacitors can be classified as electrochemical double-layer capacitors (EDLCs) and pseudocapacitors [5,6]. Moreover, these two mechanisms may function simultaneously based on the nature of the materials. Generally, carbon based materials including activated carbon, porous carbon and carbon nanotubes are used in EDLCs [7–9].

Graphene, a kind of two-dimensional carbon material constructed by layers of sp^2-bonded carbon atom, exhibits applications in fields of electronics [10], composite materials [11–13], catalysis [14,15], energy generation [16,17] and storage [3,5,18] etc owing to its extreme mechanical strength, high specific surface area and electrical conductivity [19–21]. The graphene produced through chemically reducing graphene oxide (GO) obtained from graphite is considered to be the more efficient, inexpensive and simple

* Corresponding author. Tel.: +86 351 7010699; fax: +86 351 7016358.
E-mail address: han_gaoyis@sxu.edu.cn (G. Han).

0378-7753/$ – see front matter © 2013 Elsevier B.V. All rights reserved.
http://dx.doi.org/10.1016/j.jpowsour.2013.11.115

approach to large-scale use [22] compared with other preparation methods [23,24]. However, the chemically reduced GO (rGO) dissolved in water will occur an irreversible coagulation, which has blocked to fabricate bulk graphene materials from rGO.

Up to date, besides the graphene powder and hydrogels prepared by hydrothermal method [2,22] and the graphene papers prepared by vacuum filtration or liquid-air assembly of GO followed reduction by reducing agent or thermal treatment [15–27], the graphene fibers, as another important graphene material have attracted the researchers' attention. Recently, the graphene fibers have been produced by several research groups [28–34] through spinning GO into concentrated NaOH solution (or other concentrated solution) and then reducing by hydroiodic acid (40 wt.%) at 80 °C or hydrothermally treating the GO in a capillary. However, most literature on graphene fibers have focused on their strength and few about their electrochemical properties especially on their properties used in high-rate capacitors.

It is well known that chemical doping and etching are other effective approach to tailor the property of graphene and greatly expand their applications [35]. Usually, the N atom is considered to be an excellent dopant because it is of comparable atomic size and contains five valence electrons available to form strong valence bonds with C atoms. Thus N atoms can be introduced into the lattice of carbon easily to tune the graphene's property [36]. Compared with other N-doping approaches performed under harsh conditions [37–40], N-doped graphene synthesized by solution-phase process is considered to be a feasible approach due to its simple, low-cost and larger-scale production [41–43]. As one of N sources, hydroxylamine possesses relative lower toxic properties than the widely-used hydrazine hydrate [44], and is rarely used as the chemical reductant and dopant to prepare N-doped graphene [45].

In this paper, we develop an easy approach to prepare N-doped graphene fibers mats (NG-FMs) in large scale. The NG-FMs can be conveniently produced by continuously spinning concentrated GO suspension into the ethanol solution of hydroxylamine. During the process, the shapes of GO fibers will be fixed through the coagulating caused by hydroxylamine and the dehydrating caused by ethanol at room temperature. Finally, the desired NG-FMs are obtained after the evaporation of the solvent under heating. The NG-FMs have been characterized and their electrochemical properties have been investigated in detail. It is believed that this methodology provides a simple and convenient route to produce NG-FMs in large scale and expected that the obtained materials have highly electrochemical performance.

2. Experimental section

2.1. Materials

Natural graphite powder (325 mesh) was purchased from Tianjin Guangfu Research Institute. Hydroxylamine hydrochloride was obtained from Tianjin North Fine Chemical Co., Ltd. The single-walled carbon nanotubes (SWCNTs) were purchased from Chengdu institute of organic chemistry of Chinese Academy Sciences and treated in mixed acid of H_2SO_4 and HNO_3 (3:1 in volume), the multi-walled carbon nanotubes (MWCNTs) were obtained from department of chemical engineering of Tsinghua University and fluxed in mixed acid of H_2SO_4 and HNO_3 (3:1 in volume) for 20 min [46]. All other chemicals used in this study were of analytical grade. GO was prepared by oxidation of natural graphite powder according to the method reported in literature [13,25]. Hydroxylamine was generally prepared through the reaction of equal molar hydroxylamine hydrochloride with potassium hydroxide in ethanol solution and used instantly. Briefly, 2.0 mL ethanol solution of hydroxylamine (35 mg mL^{-1}) and 1.0 mL ethanol solution of KOH (56 mg mL^{-1}) were mixed and reacted for 30 min at room temperature, then the mixture was centrifugated at 12,000 r min^{-1} for 3 min to remove the deposition. The ethanol solution of hydroxylamine with a concentration of 11 mg mL^{-1} was reserved for use.

2.2. Fabrication of NG-FMs

The concentrated dispersion of GO (12.0 mg mL^{-1}) was spinned into the ethanol solution of hydroxylamine (0.5 mg mL^{-1}) through a micro-nozzle with a diameter of about 50 microns, and the shape of GO fibers was fixed during the spinning process. After the wet spinning process was finished and the fibers were placed at room temperature for several hours, the solution was then heated at 70 °C for 4.0 h to evaporate the remaining ethanol solution of hydroxylamine from the container. Finally, the NG-FM100 was obtained after heating at 100 °C for 10 h. Part of the NG-FM100 was heated at 300 °C for 2 h, and then the NG-FM300 was obtained after the mat was washed by distilled water and dried. For comparison, the films of SWCNTs and MWCNTs have also been fabricated through filtering the dilute dispersion (0.2 mg mL^{-1}) of the corresponding carbon nanotubes (CNTs).

2.3. Fabrication of the capacitors

The fabrications of the capacitors were described as follows: two pieces of nearly identical (in weight and size) NG-FMs were separated by a filter paper soaked with 25% KOH aqueous solution. Before the electrochemical measurements, the slices of NG-FMs were also immersed in electrolyte solution under vacuum in order to make the electrolyte filled in interior. Two Pt foils were used as the current collectors. All the components were assembled into a sandwiched structure between the two plastic sheets and the structural scheme of the capacitor was showed in Fig. S1.

2.4. Characterization and measurement

The XRD patterns of the samples were recorded on a Bruker D8 Advance X-ray diffraction meter with Cu Kα radiation and graphite monochromator at the scan speed of 5° min^{-1} with a step size of 0.02°. The morphologies of the samples were observed by using a JEOL-JSM-6701 field-emission microscope (SEM) operating at an accelerating voltage of 10 kV. X-ray photoelectron spectroscopy (XPS) measurements were performed with an ESCAL-ab 220i-XL spectrometer (VG Scientific, England) using a monochromic Al Ka source at 1486.6 eV. Raman spectra were recorded on a JobinYvon Lab RAMHR800 microscopic confocal Raman spectrometer by using laser of 514 nm as incident light. Nitrogen adsorption measurements were performed at 77 K on a Micromeritics ASAP 2000 volumetric adsorption system. The specific surface area of the samples was calculated using the Brunauer–Emmett–Teller (BET) equation, while the size distributions of pores were estimated by the Barrett–Joyner–Halenda (BJH) method from adsorption and desorption branches of the isotherms.

Electrochemical performances of the cells were tested by cyclic voltammetry (CV), galvanostatic charge/discharge and electrochemical impedance spectroscopy (EIS) on a CHI660C electrochemistry workstation (Chenhua, Shanghai). EIS tests were carried out in the frequency range of 10^5–10^{-2} Hz at the amplitude of 5 mV referring to open circuit potential. In order to analyze the variation of capacitance with varying scanning rates, the specific capacitance (C_{sc}) of the electrodes can be calculated based on CV curves [45] according to following equation:

$$C_{sc} = \left(\int IdV\right) \Big/ (\upsilon m \Delta V) \quad (1)$$

Where I is the response current (A), ΔV the difference of potential during the CV tests (V), υ the potential scan rate ($V\ s^{-1}$), and m the mass of one electrode (g).

Furthermore, the C_{sc}, power density and energy density can also be calculated from the galvanostatic charge/discharge curves [47]. For example, the C_{sc} can be obtained by using the equation:

$$C_{cs} = 2(I\Delta t/m\Delta V) \quad (2)$$

Where I represents the constant discharge current, Δt the discharging time, m the mass of one electrode, and ΔV the voltage drop upon discharging. Then the energy density and power density of the EDLCs depicted in the Ragone plot can be calculated by using the equations:

$$E = (1/8)C_{cs}\Delta V^2 \quad (3)$$

$$P = E/\Delta t \quad (4)$$

3. Results and discussion

As shown in Fig.1, concentrated GO suspension is continuously spinned into the bottom of the container filled with ethanol solution of hydroxylamine which acts as a coagulant, N-source and reducer during the process of preparation (Fig. S2). With the mutual diffusion of water and ethanol, hydroxylamine molecules diffuse into the GO fibers gradually and interact with GO. Then the shapes of GO fibers are fixed when the GO sheets are coagulated by hydroxylamine and the water in GO fibers is dehydrated by ethanol. Finally, the NG-FMs will be obtained easily after evaporating the solvent at heating.

The used GO in this work contains a relatively high O content (33.1% in atom, Fig. S3) and high content of defects and sp^3 type carbon (Fig. S4). The fibers in NG-FMs prepared by spinning 12 mg mL^{-1} GO suspension and followed by thermally treating have the diameter of about 10–20 μm and the surface is very coarse (Fig. 2A). The magnified image shows that the surface of NG-FMs is formed by the rugate graphene sheets with a voile-like structure. From the SEM image of the fiber's transverse section (Fig. S5), it is found that the interior of the NG-FM is porous too. It is also found that the films of SWCNTs and MWCNTs show very coarse surface and the porous structure (Fig. S6). Compared with the film of SWCNTs, the film of MWCNTs possesses larger pores because SWCNTs bundles are easily formed. NG-FM (17 × 17 cm) (Fig. 2B and Fig. S7) are flexible and can be folded into small blocks (the insert in Fig. 2B) without damaging their structure. The nitrogen adsorption–desorption isotherms of NG-FM (Fig.2C) reveal a typical characteristic of Type IV isotherm. Multilayer adsorption that takes place at lower pressures is followed by the capillary condensation at the relative pressures range of 0.63–0.90. Adsorption–desorption isotherm for smaller pores is reversible, but a serious hysteresis in the isotherm is observed in the range of large pores, which indicates the characteristic of pores with large interior space and small entrances [48,49]. The specific surface areas are determined to be about 176.0 and 192.4 $m^2\ g^{-1}$ based on BET method and the total pore volumes to be 0.21 and 0.17 $cm^3\ g^{-1}$ for NG-FM300 and NG-FM100 according to the adsorption–desorption isotherms, respectively. From the average pore diameter calculated according to the BJH method shown in Fig. 2D, it is found that NG-FM100 exhibits larger pore volume than NG-FM300 in small pore diameter range. However, NG-FM300 shows larger volume than NG-FM100 in the large pore diameter range due to the delimination of some groups on graphene at higher treating temperature.

As a powerful tool to identify the elements' states in material, XPS is used to characterize the elements composition of NG-FMs. The GO shows obvious C and O peaks but no N signal in the XPS spectrum (Fig. 3A-a). However, there are clear N signals in the XPS spectra corresponding to NG-FM100 and NG-FM300 (Fig.3A-b and c). Compared with the GO, the peaks corresponding to C–O bonds become weaker for NG-FMs (Fig. S8 and Table S1). Similar to our result reported previously [45] in which the reaction is carried out under solvothermal at 150 °C, it is found that N atoms have doped into the graphene sheets, which may indicate that the hydroxylamine is an effective and convenient N-doping and reducing agent for GO at relatively low temperature. The elemental analysis based on XPS data shows that the GO, NG-FM100 and NG-FM300 possess the C/O ratio of 2.06, 4.70 and 8.31, respectively. The content of N in NG-FM100 and NG-FM300 is calculated to be about 3.2 and 2.19% in atom. These results reveal that the N atoms have been successively doped into the graphene sheets, and that GO can be effectively reduced by hydroxylamine at low temperature of 100 °C and heating at high temperature can increase the C/O ratio dramatically. In order to investigate the possible types of N inserted in the NG-FMs, the high-resolution N1s XPS spectra of the products prepared at different temperatures are collected in Fig. 3B. Generally, the peaks located at 398.4, 400.0, and 401.7 eV are assigned to pyridinic-, pyrrolic-, and quaternary-type of N which includes the N doped in the graphene structure and the N in group of $R-NH_3^+$, respectively [35,50]. The content of various N species is quantitatively depicted in Table 1, which shows that with the increase of the temperature of thermal treatment, the proportion of quaternary- and pyrrolic-type of N decreases while the content of pyridinic N remarkably increases. The possible N insertion pathway in the graphene sheets is thought to be similar to the literature reported previously [45]

Fig.4 displays the XRD patterns of GO, NG-FM100 and NG-FM300, it is clear that the XRD pattern of GO shows two diffraction peaks at 11.1 and 21.4° which correspond to the interplanar spacing of 7.96 and 4.15 Å according to the Bragg equation ($2d\sin$

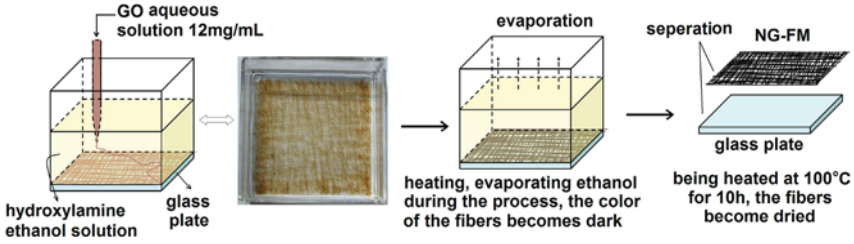

Fig. 1. The schematic diagram of the process for preparation of NG-FMs.

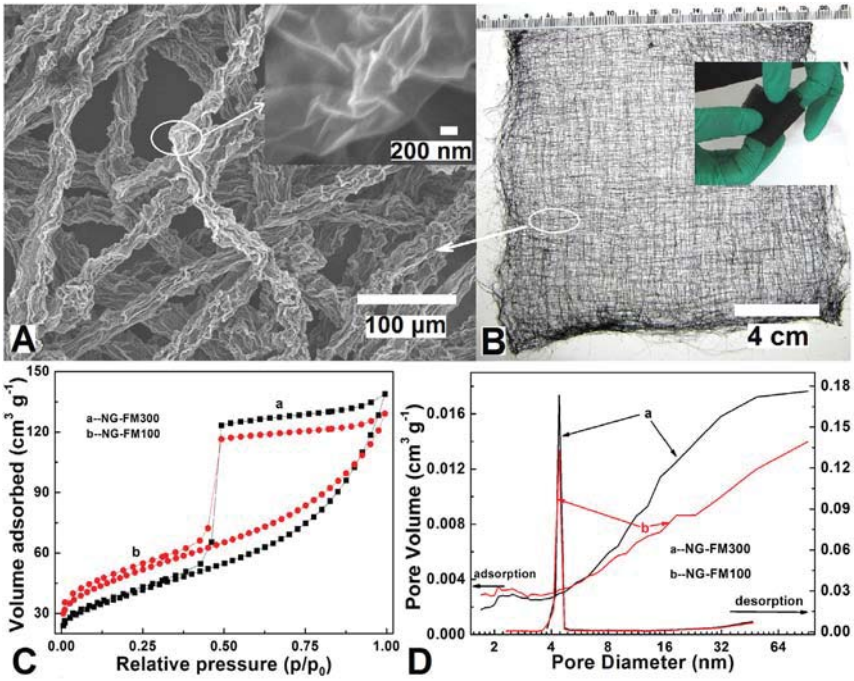

Fig. 2. The SEM image (A) and the photograph of the mat of NG-FM100 (B, the insertion is its folded block), the nitrogen adsorption and desorption isotherms of NG-FM300 (C-a) and NG-FM100 (C-b) at 77 K, the corresponding pore size distribution curves, estimated from adsorption and desorption branch of N_2 isotherms by BJH method for NG-FM300 (D-a) and NG-FM100 (D-b).

$\theta = n\lambda$). However, the peak at 11.1° has entirely disappeared after the GO are transferred to NG-FMs, while a broad diffraction peak located at 24.5° is observed in the NG-FM100, which indicates that the interplanar distance between the graphene layers has become small due to the decrease of the oxygen-containing groups. The distance between the layers is calculated to be about 3.63 Å and is still larger than that of graphite (3.35 Å) although it is much smaller than that of GO. Furthermore, it is interesting to find that the diffraction peak for NG-FM300 does almost not shift compared with that for NG-FM100, indicating that the layer spacing between the graphene sheets has not change although the NG-FM has been thermally treated at 300 °C. This may be attributed to the miscellaneous arrangement of GO sheets during the spinning process and the quick gelation of the thin fibers caused by the hydroxylamine. The electrical conductivity of single fiber is measured by four-point method to be about 1.8 S cm^{-1} for the sample of NG-FM100 and 21.0 S cm^{-1} for NG-FM300.

CV method has been used to characterize the capacitor cells assembled by the NG-FMs and the results are shown in Fig. 5. The CV curves of the as-assembled capacitors of NG-FM100, NG-FM300, films of SWCNTs and MWCNTs measured in 25% KOH aqueous electrolyte exhibit rectangular-like shapes without obvious redox peaks, indicating an ideal capacitive behavior (Figs. S9 and S10). From Fig.5A and B, it is found that the CV profiles of the cell assembled by NG-FM300 show a good rectangular shape at scan rate of 500 mV s^{-1} and 1.0 V s^{-1}. Moreover, the CV profiles still retain relatively rectangular shape without obvious distortion even at scan rate as high as 8.0 V s^{-1} (Fig. 5C). However, the capacitors assembled by NG-FM100 only show the CV profiles with relatively good rectangular shape below the scan rates of 1.0 V s^{-1}. It is interesting to find that the capacitors fabricated by SWCNTs and MWCNTs electrodes also show good rectangular CV profiles compared with NG-FM300, and that MWCNTs exhibit relatively larger current density than SWCNTs at the same current density. However, the current densities of the cells assembled by CNTs are much smaller than that of NG-FMs at the same scan rates. It can be also found that NG-FM300 shows larger current density than that of NG-FM100 at the same scan rates, indicating that NG-FM300

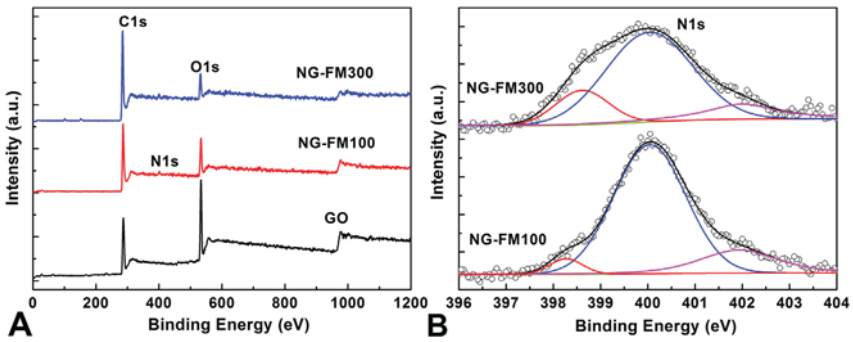

Fig. 3. The general XPS spectra of GO, NG-FM100 and NG-FM300 (A) and the high resolution N1s XPS spectra of NG-FM100 and NG-FM300 (B).

Table 1
The contents of different type of N in NG-FM100 and NG-FM300 based on XPS.

The type of N atom	NG-FM100		NG-FM300	
	Binding energy (eV)	Content (at.%)	Binding energy (eV)	Content (at.%)
Pyridinic N	398.26	4.32	398.64	16.49
Pyrrolic N	400.05	77.80	400.06	69.56
Quaternary N	401.96	17.89	402.02	13.95

possesses the desirable fast charge/discharge property for power devices. The C_{cs} of the electrodes (single electrode) can be calculated based on the CV profiles, and it is found that NG-FM300 and NG-FM100 have the similar C_{sc} values of about 188 and 177 F g^{-1} at low scan rate of 5.0 mV s^{-1}, respectively. The SWCNTs and MWCNTs have almost the same C_{sc} values of about 40 F g^{-1}, which is consistent to the result reported previously [51]. Considering that the volumetric capacitance is other important parameter for practical use, therefore the volumetric capacitance values are estimated to be about 75.2 (NG-FM300), 74.7 (NG-FM100), 32.0 (SWCNTs) and 25.6 F cm^{-3} (MWCNTs) based on the bulk density of NG-FM100 (0.422 g cm^{-3}), NG-FM300 (0.40 g cm^{-3}), SWCNTs (0.801 g cm^{-3}) and MWCNTs (0.639 g cm^{-3}). The C_{sc} values of all the materials decrease with the increment of the scan rates, but the trend of decrease for NG-FM300 is much slighter than that for NG-FM100, and the trend of decrease for MWCNTs is slighter than that of SWCNTs. For example, the C_{cs} value of the NG-FM300 can retains 74.2% (140 F g^{-1}) and 48.4% (91 F g^{-1}) of the initial C_{cs} at high scan rate of 1.0 and 10.0 V s^{-1} (Fig. 5D-a), which is much better than many previously reported carbon materials [52–55]. However, the C_{cs} value of the NG-FM100 can only retains 56.4% (100 F g^{-1}) and 18.6% (33 F g^{-1}) of the initial C_{cs} at high scan rate of 1.0 and 10.0 V s^{-1} (Fig. 5D-b). The C_{cs} values of carbon nanotubes can retain 78% (31.4 F g^{-1}) for MWCNTs and 70% (28 F g^{-1}) for SWCNTs (28 F g^{-1}) at scan rate of 1.0 V s^{-1}, and 55.2% (22.2 F g^{-1}) for MWCNTs and 50% (20 F g^{-1}) for SWCNTs at scan rate of 10 V s^{-1} (Fig. 5D-c and d). But the retained C_{cs} values of carbon nanotubes are much smaller than NG-FMs at all measured scan rates. The C_{cs} of EDLCs is related not only to the specific surface area, microstructure and hetero atom content of the materials of electrodes but also the ion-transport capability. The pore size distribution is one key factor for the C_{cs} of the materials of electrodes. For example, though activated carbons possess large specific surface area and abundant micropores, their C_{cs} does not give a clear dependence on specific surface area [56,57] and still suffer from capacitance degradation owing to lagged ion transport within their closed or tortuous pore structure [57,58]. On the other hand, the pyridinic type of N plays an important role for the improved capacitances for all electrolytes and the pyrollic type of N can improve the capacitance further when negatively charged in basic conditions and that the presence of quaternary-type of N can improve the conductivity of graphene [59]. Here, the NG-FM100 and NG-FM300 contain 17.5 and 10.7% O in atom, and 3.20 and 2.19% N in atom based on the XPS data, and furthermore they possess mainly the mesopores and macropores according to the N_2 adsorption–desorption isotherms. Therefore, the NG-FMs have relatively larger C_{cs} although their specific surface area is lower compared with activated carbons whose surface area mainly comes from its micropores. It should be notable that the carbon nanotubes have small C_{sc} due to SWCNTs' bundling and MWCNTs' multilayer or insufficient porosity resulting in reduced electrolyte accessible surface area [51]. The NG-FM300 has better capacitive performance compared with NG-FM100, which may be because that the improved conductivity of NG-FM300 and the large pores can accelerate the charge-transfer and the diffusion of electrolyte during the CV progress at high scan rate [45].

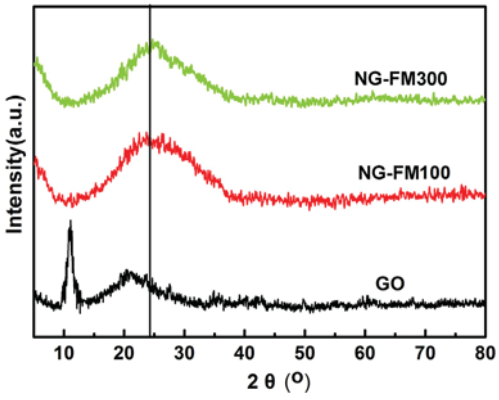

Fig. 4. The XRD patterns of GO, NG-FM100 and NG-FM300.

The charge/discharge curves of the cells prepared by NG-FMs and carbon nanotubes show the symmetrical triangles of the charge/discharge plots with small *iR* drop when the current densities are lower than 20.0 A g^{-1}, indicating the capacitors exhibit small inner resistance (Figs. S11 and S12). Fig. 6 show the typical galvanostatic charge/discharge curves of the cell assembled by electrodes of NG-FM100, NG-FM300, SWCNTs and MWCNTs at large current densities of 100, 150, 200 and 250 A g^{-1}, respectively. It is found that the *iR* drop increases with the increase of the current density from 100 to 250 A g^{-1} for all the materials. Moreover, it is clear that the cell prepared by NG-FM300 (Fig. 6B) displays a lower *iR* drop at the beginning of the discharge process and a longer discharged time than that by NG-FM100 (Fig. 6A), MWCNTs (Fig. 6D) and SWCNTs (Fig. 6C). The *iR* drop is usually caused by the internal resistance of the devices and the migration rate of the ions in electrolyte. Commonly, the capacitors using organic solution as electrolyte exhibit large *iR* drop compared with the aqueous electrolyte [60] at the same current density due to the low migration rate of the ions in organic solution. Therefore, the capacitors fabricated by NG-FMs carbon nanotubes in aqueous solution of KOH show the small *iR* drop. The low inner resistance is of great importance in energy-storing devices as less energy will be wasted to produce unwanted heat during charging/discharging processes. These results reveal that NG-FM300 exhibits not only small *iR* drop but also large C_{cs}, and indicate it exhibits a rapid current response and excellent capacitive behavior and it is more suitable for fabricating safe and power-saving supercapacitors.

The repeated charge/discharge curves (Fig. 7A) of the cell of NG-FM300 at current density of 10 A g^{-1} show a less deviation from the cutoff potential of 0.80 and −0.20 V, revealing that the cell has good stability. In order to validate the promising applications of the NG-FMs in electrochemical capacitors, the Ragone plots of the symmetric capacitors based on the data of the discharged curves are shown in Fig. 7B. It is found that the energy densities slowly become small with the increment of power density and the energy densities of the cell fabricated by NG-FM300 at the same power density are higher than that by NG-FM100, MWCNTs and SWCNTs. For example, the capacitors assembled by NG-FM300 (Fig. 7B-a) can exhibit an energy density of 5.75 Wh kg^{-1} at the power density of 249.7 W kg^{-1} at discharged current density of 1.0 A g^{-1} and 2.24 Wh kg^{-1} at 48.7 kW kg^{-1} at discharged current density of 300 A g^{-1} (excluding the *iR* drops). The capacitors prepared by NG-FM100 (Fig. 7B-b) possesses energy densities of 5.25 and 1.37 Wh kg^{-1} at the power density of 249.6 W kg^{-1} and 39.8 kW kg^{-1} at the discharged current density of 1.0 and 300 A g^{-1}. However, the capacitors fabricated by carbon nanotubes (Fig. 7B-c

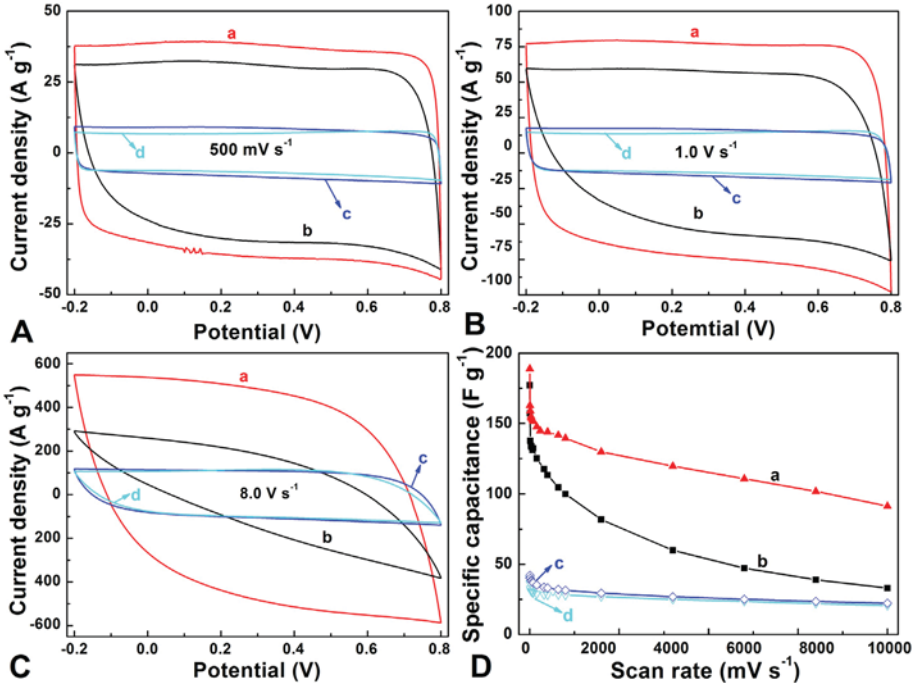

Fig. 5. The CV curves of the cells assembled by different materials at different scan rates (A–C), and the plots of the specific capacitance versus the scan rates (D). Curves a, b, c and d are corresponding to the curves for NG-FM300, NG-FM100, MWCNTs and SWCNTs, respectively.

and d) possess much smaller energy densities than that by NG-FMs at the same power densities due to the low C_{cs} of CNTs. These results are better than the power target of the Partnership (15.0 kW kg^{-1}) for a New Generation of Vehicles [61].

The kinetic feature of the ion diffusion in the NG-FMs is also investigated by using EIS technique. Fig. 8A and C show the Nyquist plot obtained at the frequency-range of 10^5–10^{-2} Hz (the inserted figure shows the high-frequency region). At very high frequency, the intercept on real axis represents a combined resistance including intrinsic resistance of electrode materials, ionic resistance of electrolyte and contact resistance between electrode and current collector [62,63]. It is also found that all the capacitors have small overall internal resistance, indicating that there are good electrodes contacts. The negligible high-frequency resistor-capacitor loops for the capacitors of NG-FM300, SWCNTs and MWCNTs reveal the charge-transfer resistances are small. However, the

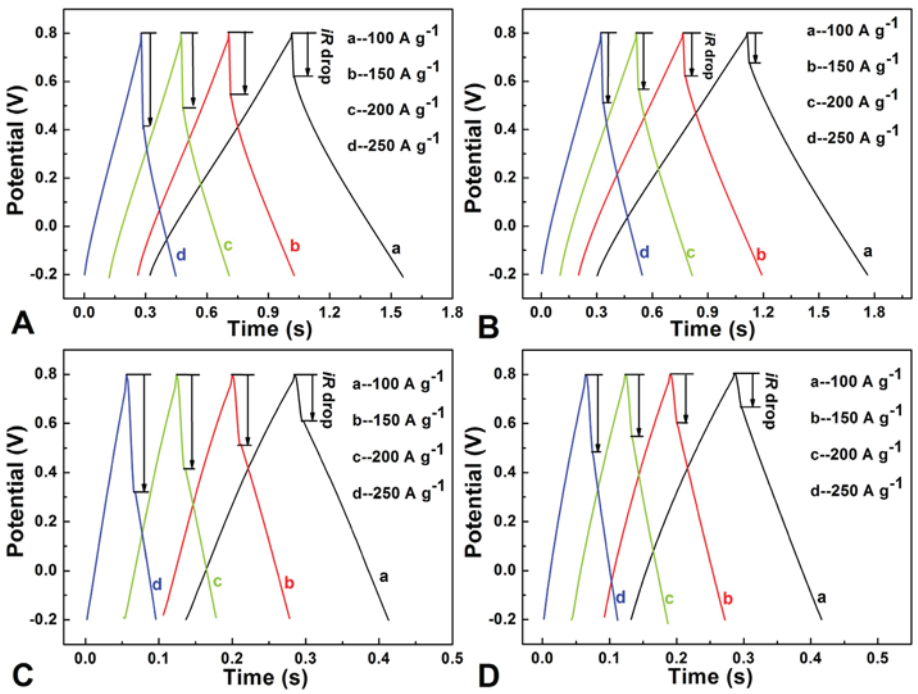

Fig. 6. The charge/discharge curves at different current density for the cell assembled by NG-FM100 (A), NG-FM300 (B), SWCNTs (C) and MWCNTs (D).

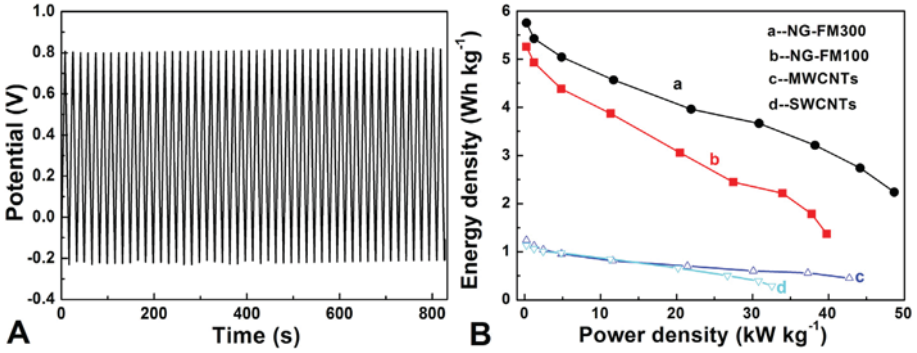

Fig. 7. The repeated charge/discharge curves of the capacitor assembled by NG-FM300 and at 10 A g^{-1} (A), and the Ragone plots of the cells (B) assembled by NG-FMs (a, b) and CNTs (c, d).

capacitor of NG-FM100 shows a larger charge-transfer resistance compared with other. Furthermore, it is also found that the impedance frequency for the finish of the charge-transfer process in capacitors of NG-FM300 (1172 Hz), SWCNTs (810 Hz) and MWCNTs (1500 Hz) is much higher than that of NG-FM100 (47 Hz) [64], indicating that NG-FM300 exhibits much better high-rate capacitive properties than NG-FM100. Fig. 8B and D present the plots of the phase angles versus the frequency of the capacitors assembled by NG-FMs and CNTs. The f_0 can provide a time constant τ_0 ($1/f_0$) which tells how fast the device can be reversibly charged and discharged [65]. It is easy to find that the τ_0 for capacitors of NG-FM300, MWCNTs and SWCNTs is about 0.061, 0.043 and 0.072 s respectively, which is much smaller than that of NG-FM100's electrodes (0.45 s). It should be noted that the τ_0 for most commercially available electrochemical capacitors including those specially designed for high power applications is slightly smaller than 1.0 s [47]. These characters indicate that the NG-FM300 could be developed into the good electrode materials with the high-rate capacitive ability.

As the service life is a very important factor for the electrode of electrochemical capacitor, so the stabilities of the cells assembled by electrodes of NG-FM have been evaluated by using CV method at a scan rate of 80 mV s^{-1}. As can be seen, the CV curve recorded at 4500th has only a tiny pattern change compared with the 1st CV profile for both the materials (Fig. 9A). Furthermore, it is found from Fig. 9B that the C_{cs} value has almost not changed during the whole cyclic tests. Initially, the C_{cs} for NG-FM300 electrodes has some slight increase, but it tends to keep stable at the successive test period, only less than 1% fluctuation for C_{cs} is observed during the test. However, the C_{cs} for NG-FM100 still remained about 95% after 4500 cyclic CV charge/discharge process. These results illustrate that the material of NG-FMs especially NG-FM300 exhibits good durability and may be developed as a suitable material for high-rate handling electrochemical capacitors applications.

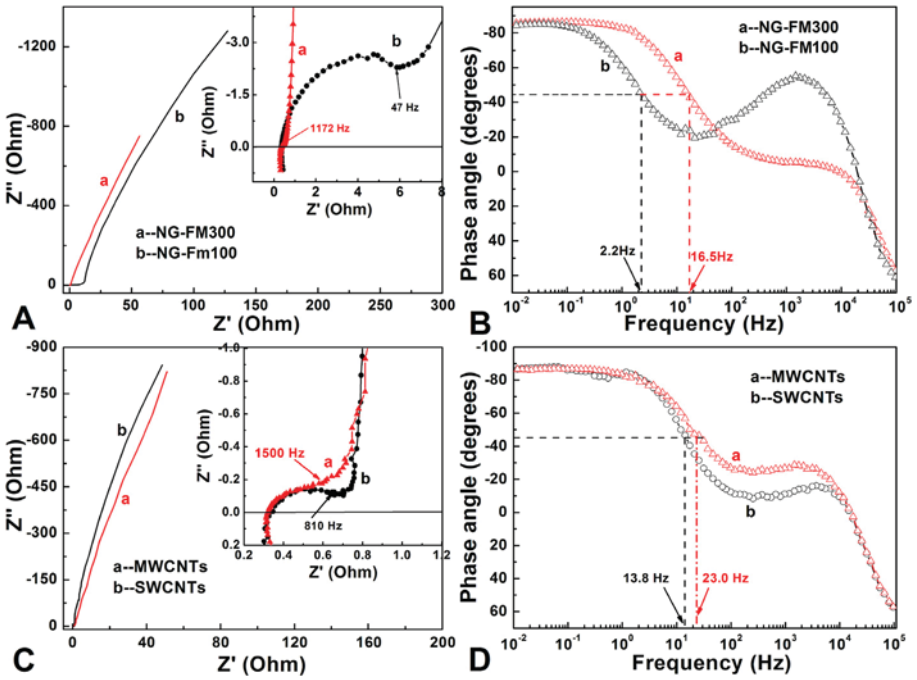

Fig. 8. The EIS of the cell assembled by the NG-FMs (A) and CNTs (C, the insertion is the region of high-frequency part), the plots of phase angles versus the frequency for cell of NG-FMs (B) and CNTs (D).

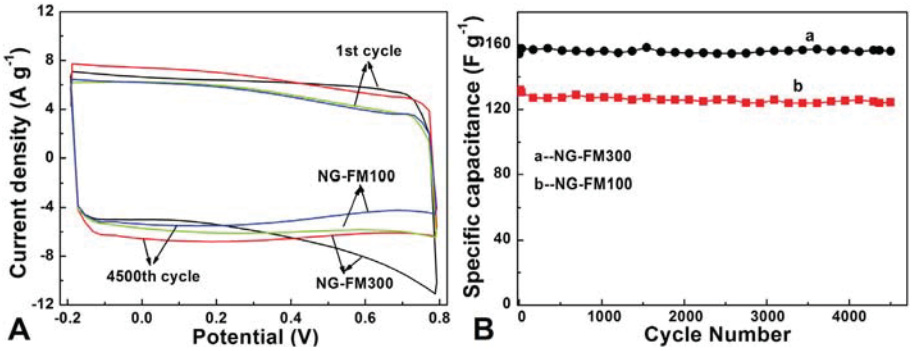

Fig. 9. The CV curves recorded at 1st and 4500th (A) for the cells assembled by NG-FMs, and the cyclic stability of the NG-FMs electrode (B) upon repeated scans at 80 mV s^{-1}.

4. Conclusion

The NG-FMs have been prepared by combining wet spinning and thermal treatment, and exhibit relatively large specific surface area and porous structure with large interior and small entrance. The fiber mats can be easily obtained in large scale and are flexible. The thermal treatment at relatively high temperature can increase the sample's electrical conductivity. Electrochemical measurements show that the capacitor assembled by NG-FM300 has a power density 48.7 kW kg^{-1} at discharged current density of 300 A g^{-1}, and that NG-FM300 has the high-rate capability and possesses C_{cs} of about 188 F g^{-1}, may be developed as new high-performance material for supercapacitors.

Acknowledgments

We appreciate funding from National Natural Science Foundation of China (21274082 and 21073115) and Shanxi province (2012021021-3), and the Program for New Century Excellent Talents in University (NCET-10-0926).

Appendix A. Supplementary data

Supplementary data related to this article can be found at http://dx.doi.org/10.1016/j.jpowsour.2013.11.115

References

[1] L.L. Zhang, X.S. Zhao, Chem. Soc. Rev. 38 (2009) 2520.
[2] S. Aricò, P. Bruce, B. Scrosati, J. Tarascon, W.V. Schalkwijk, Nat. Mater. 4 (2005) 366.
[3] Y.C. Bai, R.B. Rakhi, W. Chen, H.N. Alshareef, J. Power Sources 233 (2013) 313.
[4] J.W. Lang, L.B. Kong, W.J. Wu, Y.C. Luo, L. Kang, Chem. Commun. (2008) 4213.
[5] Y. Chen, X. Zhang, P. Yu, Y.W. Ma, J. Power Sources 195 (2013) 3031.
[6] M. Inagaki, H. Konno, O. Tanaike, J. Power Sources 195 (2010) 7880.
[7] A.G. Pandolfo, A.F. Hollenkamp, J. Power Sources 157 (2006) 11.
[8] K.H. An, W.S. Kim, Y.S. Park, J.M. Moon, D.J. Bae, S.C. Lim, Y.S. Lee, Y.H. Lee, Adv. Funct. Mater. 11 (2001) 387.
[9] V. Khomenko, E. Raymundo-Pinero, F. Beguin, J. Power Sources 195 (2010) 4234.
[10] K.S. Novoselov, A.K. Geim, S.V. Morozov, D. Jiang, Y. Zhang, S.V. Dubonos, I.V. Grigorieva, A.A. Firsov, Science 306 (2004) 666.
[11] S. Stankovich, D.A. Dikin, G.H.B. Dommett, K.M. Kohlhaas1, E.J. Zimneyl, E.A. Stach, R.D. Piner, S.T. Nguyen, R.S. Ruoff, Nature 442 (2006) 282.
[12] Y.Y. Liu, G.Y. Han, Y.L. Li, M. Jin, Mater. Lett. 65 (2011) 1885.
[13] D.Y. Fu, G.Y. Han, Y.Z. Chang, J.H. Dong, Mater. Chem. Phys. 132 (2012) 673.
[14] E. Yoo, T. Okata, T. Akita, M. Kohyama, J. Nakamura, I. Honma, Nano Lett. 9 (2009) 2255.
[15] Y.Z. Chang, G.Y. Han, M.Y. Li, F. Gao, Carbon 49 (2011) 5158.
[16] X. Wang, L.J. Zhi, K. Mullen, Nano Lett. 8 (2008) 323.
[17] W.J. Hong, Y.X. Xu, G.W. Lu, C. Li, G.Q. Shi, Electrochem. Commun. 10 (2008) 1555.
[18] M.D. Stoller, S.J. Park, Y.W. Zhu, J.H. An, R.S. Ruoff, Nano Lett. 8 (2008) 3498.
[19] C. Lee, X.D. Wei, J.W. Kysar, J. Hone, Science 321 (2008) 385.
[20] A.S. Mayorov, R.V. Gorbachev, S.V. Morozov, L. Britnell, R. Jalil, L.A. Ponomarenko, P. Blake, K.S. Novoselov, K. Watanabe, T. Taniguchi, A.K. Geim, Nano Lett. 11 (2011) 2396.
[21] A.A. Balandin, Nature Mater. 10 (2011) 569.
[22] H. Bai, G.Q. Shi, Adv. Mater. 23 (2011) 1089.
[23] P.W. Sutter, J.I. Flege, E.A. Sutter, Nat. Mater. 7 (2008) 406.
[24] K.S. Kim, Y. Zhao, H. Jang, S.Y. Lee, J.M. Kim, K.S. Kim, J.H. Ahn, P. Kim, J.Y. Choi, B.H. Hong, Nature 457 (2009) 706.
[25] Y.X. Xu, H. Bai, G.W. Lu, C. Li, G.Q. Shi, J. Am. Chem Soc. 130 (2008) 5856.
[26] C. Chen, Q.H. Yang, Y. Yang, W. Lv, Y. Wen, P.X. Hou, M. Wang, H.M. Cheng, Adv. Mater. 21 (2009) 3007.
[27] C. Valles, J.D. Nunez, A.M. Benito, W.K. Maser, Carbon 50 (2012) 835.
[28] Z. Xu, C. Gao, Nat. Commun. 2 (2011) 571.
[29] Z.L. Dong, C.C. Jiang, H.H. Cheng, Y. Zhao, G.Q. Shi, L. Jiang, L.T. Qu, Adv. Mater. 24 (2012) 1856.
[30] H.P. Cong, X.C. Ren, P. Wang, S.H. Yu, Sci. Rep. 2 (2012) 613.
[31] X.Z. Hu, Z. Xu, C. Gao, Sci. Rep. 2 (2012) 767.
[32] J. Carretero-González, E. Castillo-Martínez, M. Dias-Lima, M. Acik, D.M. Rogers, J. Sovich, C.S. Haines, X. Lepró, M. Kozlov, A. Zhakidov, Adv. Mater. 24 (2012) 5695.
[33] Z. Xu, Y. Zhang, P.G. Li, C. Gao, ACS Nano 6 (2012) 7103.
[34] Z. Xu, H.Y. Sun, X.L. Zhao, C. Gao, Adv. Mater. 25 (2013) 188.
[35] H.B. Wang, T. Maiyalagan, X. Wang, ACS Catal. 2 (2012) 781.
[36] Y. Wang, Y.Y. Shao, D.W. Matson, J.H. Li, Y.H. Lin, ACS Nano 4 (2010) 1790.
[37] D. Wei, Y. Liu, Y. Wang, H. Zhang, L. Huang, G. Yu, Nano Lett. 9 (2009) 1752.
[38] C.H. Zhang, L. Fu, N. Liu, M.H. Liu, Y.Y. Wang, Z.F. Liu, Adv. Mater. 23 (2011) 1020.
[39] L.S. Panchakarla, K.S. Subrahmanyam, S.K. Saha, A. Govindaraj, H.R. Krishnamurthy, U.V. Waghmare, C.N.R. Rao, Adv. Mater. 21 (2009) 4726.
[40] D.S. Geng, Y. Chen, Y.G. Chen, Y.L. Li, R.Y. Li, X.L. Sun, S. Ye, S. Knights, Energy Environ. Sci. 4 (2011) 760.
[41] D.H. Long, W. Li, L.C. Ling, J. Miyawaki, I. Mochida, S.H. Yoon, Langmuir 26 (2010) 16096.
[42] L.F. Lai, L.W. Chen, D. Zhan, L. Sun, J.P. Liu, S.H. Lim, C.K. Poh, Z. Shen, J. Lin, Carbon 49 (2011) 3250.
[43] L. Sun, L. Wang, C.G. Tian, T.X. Tan, Y. Xie, K.Y. Shi, M.T. Li, H.G. Fu, RSC Adv. 2 (2012) 4498.
[44] D. Li, M.B. Muller, S. Gilje, R.B. Kaner, G.G. Wallace, Nat. Nanotechnol. 3 (2008) 101.
[45] Y.Z. Chang, G.Y. Han, J.P. Yuan, D.Y. Fu, F.F. Liu, S.D. Li, J. Power Sources 238 (2013) 492.
[46] G.Y. Han, J.Y. Yuan, G.Q. Shi, F. Wei, Thin Solid Films 474 (2005) 64–69.
[47] L. Zhang, G.Q. Shi, J. Phys, Chem. C 115 (2011) 17206.
[48] J.R. Matos, M. Kruk, L.P. Mercuri, M. Jaroniec, L. Zhao, T. Kamiyama, O. Terasaki, T.J. Pinnavaia, Y. Liu, J. Am. Chem. Soc. 125 (2003) 821.
[49] T.W. Kim, R. Ryoo, M. Kruk, K.P. Gierszal, M. Jaroniec, S. Kamiya, O. Terasaki, J. Phys. Chem. B 108 (2004) 11480.
[50] C.H. Hsu, P.L. Kuo, J. Power Sources 198 (2012) 83.
[51] M.H. Ervin, B.S. Miller, B. Hanrahana, B. Mailly, T. Palacios, Electrochim. Acta 65 (2012) 37.
[52] Z.A. Qiao, B.K. Guo, A.J. Binder, J.H. Chen, G.M. Veith, S. Dai, Nano Lett. 13 (2013) 207.
[53] M.J. Zhong, E.K. Kim, J.P. McGann, S.E. Chun, J.F. Whitacre, M. Jaroniec, K. Matyjaszewski, T. Kowalewski, J. Am. Chem. Soc. 134 (2012) 14846.
[54] P.Q. Wang, D. Zhang, F.Y. Ma, Y. Ou, Q.N. Chen, S.H. Xie, J.Y. Li, Nanoscale 4 (2012) 7199.
[55] B.H. Kim, K.S. Yang, J.P. Ferraris, Electrochim. Acta 75 (2012) 325.
[56] D. Qu, H. Shi, J. Power Sources 74 (1998) 99.
[57] E. Frackowiak, Phys. Chem. Chem. Phys. 9 (2007) 1774.
[58] Z. Chen, J. Wen, C.Z. Yan, L. Rice, H. Sohn, M.Q. Shen, M. Cai, B. Dunn, Y.F. Lu, Adv. Energy Mater. 1 (2011) 551.

[59] H.M. Jeong, J.W. Lee, W.H. Shin, Y.J. Choi, H.J. Shin, J.K. Kang, J.W. Choi, Nano Lett. 11 (2011) 2472.
[60] A. Izadi-Najafabadi, T. .Yamada, D.N. Futaba, M. Yudasaka, H. Takagi, H. Hatori, S. Iijima, K. Hata, ACS Nano 5 (2011) 811.
[61] Z.J. Fan, J. Yan, T. Wei, L.J. Zhi, G.Q. Ning, T.Y. Li, F. Wei, Adv. Funct. Mater. 21 (2011) 2366.
[62] V. Khomenko, E. Raymundo-Pinero, F. Beguin, Appl. Phys. A 82 (2006) 567.
[63] J.G. Wang, Y. Yang, Z.H. Huang, F.Y. Kang, Carbon 61 (2013) 190.
[64] C. Portet, G. Yushin, Y. Gogotsi, Carbon 45 (2007) 2511.
[65] C. Ma, Y. Song, J.L. Shi, D.Q. Zhang, X.L. Zhai, M. Zhong, Q.G. Guo, L. Liu, Carbon 51 (2013) 290.